Switchable anomalous valley Hall effect in 2D antiferromagnetic system

Jiaxuan Hui, Yandong Ma,* Ying Dai, Baibiao Huang, and Xinru Li†
School of Physics, State Key Laboratory of Crystal Materials, Shandong University, Shandanan Str. 27, Jinan 250100, China

(Received 4 September 2025; accepted 20 January 2026; published 6 February 2026)

Currently, the realization and control of anomalous valley Hall effect (AVHE) in two-dimensional antiferromagnetic (AFM) systems are predominantly achieved through optical excitation, which hinders its practical applications. Here, we propose a strategy to overcome this limitation by inserting a valley-active AFM layer between two ferromagnetic (FM) semiconductor layers. Using $CrCl_3-VSiS_3-CrCl_3$ heterotrilayer as a model system, our first-principles calculations reveal that interfacial proximity coupling can introduce intrinsic sublattice-asymmetric exchange field. This field can break the *PT* symmetry and lift the spin degeneracy of valleys in the AFM layer while preserving its intrinsic valley polarization, thereby inducing a pronounced AVHE. Crucially, the sublattice-asymmetric exchange field can be reversed through flipping the magnetization orientation of the FM layers, resulting in reversible static control of AVHE without altering the AFM Néel order. These findings establish an alternative paradigm for controlling AVHE in AFM materials and advance the field of antiferromagnet-based valleytronics.

DOI: 10.1103/bdfy-8ff7

I. INTRODUCTION

Valley pseudospin, which characterizes the degenerate energy extrema at distinct momentum points in the Brillouin zone, represents a fundamental electronic degree of freedom alongside charge and spin [1–8]. Because of the large separation in momentum space, the valley degree of freedom offers a robust platform for encoding and manipulating quantum information, enabling applications such as valley-based qubits or hybrid spin-valley quantum systems for quantum computing [9–13]. Similar to charge in electronics and spin in spintronics, the use of valley for information processing generates the concept of valleytronics [8,14–17]. Valleytronics offer a promising pathway toward low-power and high-speed devices that could surpass the limitations of conventional technology [6,7,18]. Beyond devices applications, a variety of novel valley-related phenomena are observed (e.g., the valley Hall effect, anomalous valley Hall effect (AVHE), quantum valley Hall effect, and valley-polarized quantum anomalous Hall effect), establishing valley physics as a critical frontier in condensed matter physics. With the recent rise of two-dimensional (2D) materials, significant efforts have been devoted to valleytronic research in both ferromagnetic (FM) and antiferromagnetic (AFM) systems [7,19–23].

A central step for realizing valleytronics is to control the AVHE [24]. In 2D FM systems, the reversal control of AVHE can be readily accomplished by switching the magnetization orientation by applying an external magnetic field [24,25]. In contrast, the situation in 2D AFM systems is fundamentally different. In 2D AFM systems, the valley index is not an independent degree of freedom but is inherently coupled to the spin via $s\cdot\tau$ (where s denotes spin and τ represents valley pseudospin) [26]. Moreover, because of the protection of the combined *PT* (parity-time) symmetry, the magnetization in 2D AFM systems is robust to external magnetic field. In this context, the current approaches to realizing and controlling AVHE in these systems rely predominantly on optical excitation [27–29]. However, optical methods are inherently dynamic, which severely limits their potential for device applications. For overcoming this limitation and advancing antiferromagnet-based valleytronics, it is highly desirable to explore alternative, static mechanisms for controlling AVHE in 2D AFM systems.

In this work, taking $CrCl_3-VSiS_3-CrCl_3$ heterotrilayer as a model platform, we demonstrate an intriguing mechanism of controlling AVHE in 2D AFM systems. Our approach employs interfacial proximity coupling by sandwiching a valley-active AFM layer between two FM semiconductor layers. This coupling can generate intrinsic sublattice-asymmetric exchange field, which breaks the *PT* symmetry and lifts the spin degeneracy of valleys in the AFM layer while preserving its intrinsic valley polarization. As a result, a pronounced AVHE can be observed. Importantly, the sublattice-asymmetric exchange field can be reversed by inversing the magnetization orientation of the FM layers, which enables the reversible and static control of AVHE. Our study greatly enriches the research on valley physics in AFM materials.

II. RESULTS AND DISCUSSION

To set the stage, we first investigate the properties of monolayers $VSiS_3$ and $CrCl_3$. Monolayer $VSiS_3$ crystallizes in the trigonal space group P-31m (No. 162). As depicted in Fig. 1(a), each unit cell contains two V, two Si, and six S atoms. The lattice constant is optimized to be $a = 5.98$ Å. Our calculations confirm that it favors an AFM Néel state

*Contact author: yandong.ma@sdu.edu.cn
†Contact author: lixr@sdu.edu.cn

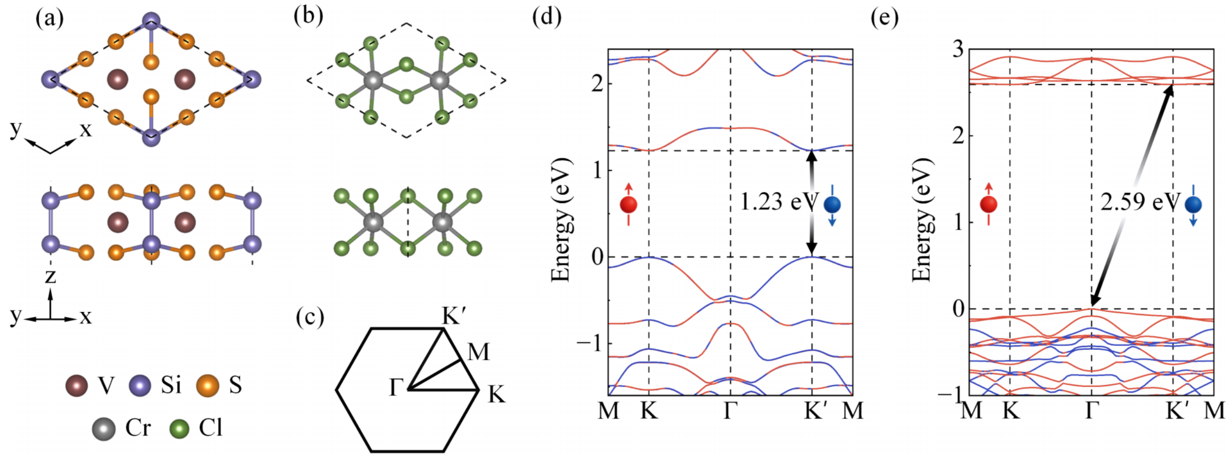

FIG. 1. (a) Crystal structure of monolayer $VSiS_3$ from top and side views. (b) Crystal structure of monolayer $CrCl_3$ from top and side views. (c) 2D Brillouin zone. (d) Band structure of monolayer $VSiS_3$ with SOC. (e) Band structure of monolayer $CrCl_3$ with SOC. The Fermi level is set to 0 eV.

as the magnetic ground state, with an energy stabilization of $\Delta E = 39.99$ meV per unit cell with respect to the FM configuration. To elucidate its electronic properties, we perform spin-resolved band structure calculations with considering spin-orbit coupling (SOC). As shown in Fig. 1(d), monolayer $VSiS_3$ exhibits semiconducting character with a band gap of 1.23 eV, which is in good agreement with previous studies [30]. Moreover, it features valley physics, with the valleys lying at the K/K' points of Brillouin zone [Fig. 1(c)]. Because of the T-symmetry breaking, the SOC introduces a valley polarization of 4.39 meV. However, the combined *PT* symmetry inherent to the monolayer strictly enforces spin degeneracy across the entire band structure. This symmetry protection precludes any spontaneous spin splitting, which is an essential prerequisite for the AVHE in this isolated layer.

Similar to monolayer $VSiS_3$, monolayer $CrCl_3$ also adopts the P-31m space group (No. 162), as shown in Fig. 1(b). Its unit cell comprises two Cr and six Cl atoms, with an optimized lattice constant $a = 6.05$ Å, in excellent agreement with prior theoretical work [31]. $CrCl_3$ exhibits a robust FM magnetic ground state, with its energy lying 37.99 meV per unit cell lower than that of its AFM state, indicating strong magnetic stability. The magnetic moment primarily originates from the Cr^{3+} ions, with each Cr atom carrying a moment of approximately 3 μ_B. Band structure calculations including SOC, presented in Fig. 1(e), reveal that monolayer $CrCl_3$ is an indirect-gap semiconductor with strong spin polarization resulting from its FM ordering. The valence band maximum (VBM) is located at the Γ point, while the conduction band minimum (CBM) resides at the K/K' points in the Brillouin zone, resulting in an indirect band gap of 2.59 eV.

Having established the fundamental properties of the constituent layers, we proceed to construct $CrCl_3-VSiS_3-CrCl_3$ heterotrilayer. It is worth emphasizing that the two constituent layers exhibit exceptionally small lattice mismatch of approximately 1.2%, which would facilitate the formation of high-quality, commensurate heterointerfaces with minimal strain. The crystal structure of $CrCl_3-VSiS_3-CrCl_3$ heterotrilayer is schematically illustrated in Fig. 2(a), where a monolayer of $VSiS_3$ is epitaxially sandwiched between two monolayers of $CrCl_3$. Fully structural optimization yields a commensurate lattice constant of 5.92 Å, representing only about 1% deviation from the average of the two parent compounds. The equilibrium interlayer spacing between $VSiS_3$ and each adjacent $CrCl_3$ layer is determined to be 3.49 Å, a value characteristic of van der Waals (vdW) bonding. Crucially, as illustrated in Fig. 2(c), the upper and lower $CrCl_3$ layers adopt fractional in-plane displacements of (1/3, –1/3, 0) and (–1/3, 1/3, 0), respectively, relative to the central $VSiS_3$ layer. These relative displacements are energetically favorable, as they effectively minimize interfacial strain and optimize interlayer vdW interactions. To assess the stability of the proposed heterotrilayer, we first confirm the dynamical stability of the constituent monolayers. The phonon spectra of both freestanding $CrCl_3$ and $VSiS_3$ monolayers, presented in Figs. S1a and S1b within the Supplemental Material [32], exhibit no imaginary modes across the entire Brillouin zone, confirming their dynamical stability. The $CrCl_3-VSiS_3-CrCl_3$ heterotrilayer is constructed from these stable monolayers and stabilized primarily by vdW interactions. To evaluate the interfacial stability, we calculate the formation energy defined as

$$E_{\text{form}} = [E_{\text{hetero}} - (E_{\text{VSiS}_3} + 2E_{\text{CrCl}_3})]/N,$$

where E_{hetero} represent the total energy of the heterotrilayer, and E_{VSiS_3} and E_{CrCl_3} denote the total energies of the corresponding freestanding monolayers in their magnetic ground states (specifically, the AFM state for $VSiS_3$ and the FM state for $CrCl_3$). N is the total number of atoms in the heterotrilayer. Adopting this normalization per atom, consistent with previous first-principles studies [33–35], facilitates direct comparison across different vdW systems. The obtained formation energy is approximately –192 meV/atom. This significant negative value indicates a thermodynamically favorable formation process and suggests strong interfacial coupling between the constituent layers. To further substantiate the stability of the $CrCl_3-VSiS_3-CrCl_3$ heterotrilayer beyond energetic considerations, we explicitly examine its dynamical stability. The phonon dispersion of the entire heterotrilayer is calculated, and the absence of imaginary phonon

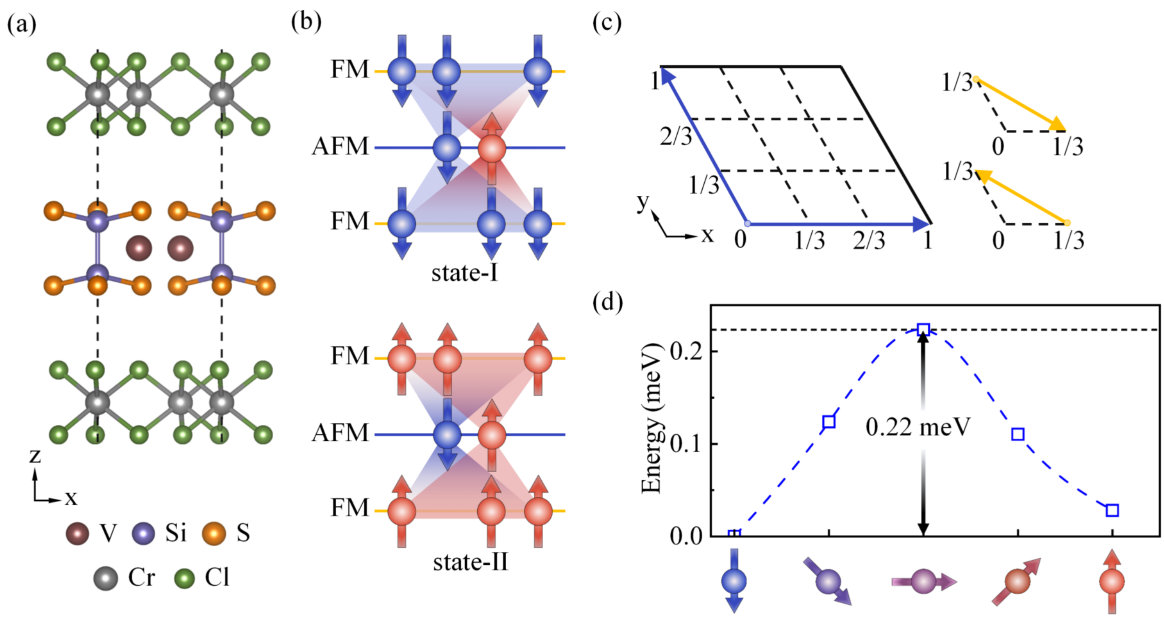

FIG. 2. (a) Crystal structure of $CrCl_3-VSiS_3-CrCl_3$ heterotrilayer from side views. (b) Schematic diagrams of state-I and state-II. (c) Schematic diagrams of in-plane displacement in heterotrilayer. (d) Energy revolution during the conversion process from state-I to state-II.

modes throughout the Brillouin zone confirms its dynamical stability, as presented in Fig. S1c within the Supplemental Material [32]. In addition to dynamical stability, we examine the thermal stability of the heterotrilayer using *ab initio* molecular dynamics (AIMD) simulations at 300 K. As illustrated in Fig. S2 within the Supplemental Material [32], the heterotrilayer maintains its structural integrity throughout the 5 ps simulation, exhibiting no significant structural distortion, bond breaking, or interlayer decoupling, confirming the thermal stability of $CrCl_3-VSiS_3-CrCl_3$.

We systematically investigate all typical stacking configurations to verify the ground-state configuration. Specifically, we calculate the energy barrier along a continuous path of relative interlayer displacements, as shown in Fig. S3a (see the Supplemental Material [32]), where the two FM $CrCl_3$ layers are shifted diagonally relative to the central AFM $VSiS_3$ monolayer. The corresponding displacements are illustrated in Fig. S3b (see the Supplemental Material [32]). Our results confirm that the stacking configuration adopted in the main text corresponds to the energetic minimum and is thus the ground state. Furthermore, to address the robustness of the observed physical effects against stacking variations, we examine the electronic structure and valley-related properties for other stacking configurations. Notably, the electronic states near the band edges, as well as the valley properties, remain almost unaffected. This supports the robustness of the sublattice-asymmetric exchange field in the $CrCl_3-VSiS_3-CrCl_3$ heterotrilayer against such structural variations. Regarding experimental feasibility, the fabrication of the $CrCl_3 - VSiS_3 - CrCl_3$ heterotrilayer lies well within the reach of established van der Waals assembly techniques. Monolayers of $CrCl_3$ and $VSiS_3$, as layered materials, can be obtained via mechanical exfoliation from their bulk crystals or synthesized through methods like physical vapor transport [36–38]. The recent advancement of deterministic transfer methods has proven highly effective in creating high-quality, custom-designed heterotrilayers with atomically clean interfaces and precise rotational alignment [39–41]. These developed protocols provide a reliable pathway for the layer-by-layer assembly of the proposed $CrCl_3-VSiS_3-CrCl_3$ heterotrilayer, making its experimental realization highly feasible.

Upon considering the magnetic phases, there are two distinct, yet energetically degenerate, magnetic configurations for the vdW heterotrilayer, referred to as state-I and state-II and schematically illustrated in Fig. 2(b). In state-I, both $CrCl_3$ layers exhibit out-of-plane FM alignment with spin-down polarization. Conversely, in state-II, both $CrCl_3$ layers exhibit out-of-plane FM alignment with spin-up polarization. Obviously, the two sublattices in $VSiS_3$ layer experience inequivalent interlayer exchange couplings with the top and bottom $CrCl_3$ layers. Such distinct coupling can generate intrinsic sublattice-asymmetric exchange field acting on the $VSiS_3$ layer. This exchange field in $VSiS_3$ layer explicitly breaks the combined *PT* symmetry that protects spin degeneracy in the freestanding $VSiS_3$ monolayer, thereby lifting the spin degeneracy at the valleys while preserving its intrinsic valley polarization. Notably, the direction of this sublattice-asymmetric exchange field is opposite in state-I and state-II. The reversibility between these two magnetic states therefore enables effective switching of the valley spin splitting, offering a viable route for controlling valley-dependent properties in the heterotrilayer.

The energy barrier separating these two states is a critical parameter governing the feasibility of magnetic switching for device applications. To evaluate this, we calculate the minimum energy path for the coherent magnetization reversal process, where the magnetic moments of Cr atoms in both layers rotate synchronously from their initial state-I orientation $(0, 0, -3)\,\mu_B$ to the final state-II orientation $(0, 0, 3)\,\mu_B$. This reversal path proceeds via an intermediate state where the moments are aligned along the in-plane x-axis direction.

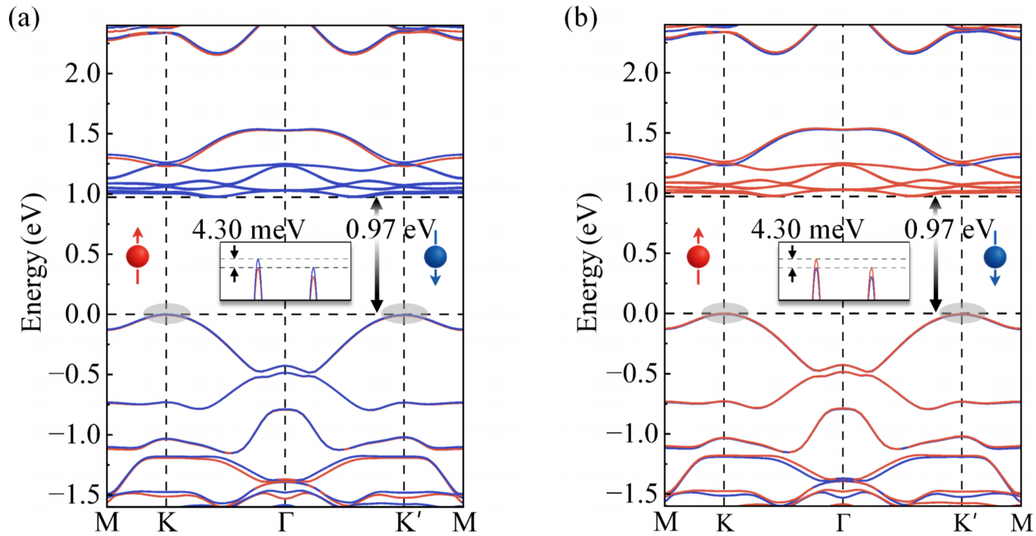

FIG. 3. Spin-resolved band structures of $CrCl_3-VSiS_3-CrCl_3$ heterotrilayer with SOC under (a) state-I, and (b) state-II. The Fermi level is set to 0 eV.

As shown in Fig. 2(d), the calculated energy barrier for magnetization switching between State-I and State-II is 0.22 meV per unit cell. The relatively small barrier suggests that thermal fluctuations could randomize the FM orientation at elevated temperatures. The switching barrier is intrinsically linked to the interfacial magnetic exchange coupling and the magnetic anisotropy energy (MAE) of the ferromagnetic layers, both of which can be optimized in material design.

Figure 3 presents the spin-resolved band structure including SOC for both states. The system retains its semiconducting character with a band gap of 0.97 eV. A key finding is that while the characteristic valley polarization of $VSiS_3$ is maintained, the spin degeneracy of valleys in $VSiS_3$ is lifted, leading to a valley spin splitting of 4.30 meV, corresponding to a thermal stability temperature of approximately 50 K, which is primarily governed by the orbital character of band edges near the K/K' points. It can be effectively enhanced through well-established external perturbations. For instance, applying external strain or electric field can effectively modulate the orbital hybridization or strengthen the SOC effects at the valleys, thereby increasing the valley polarization and spin splitting [42–45]. This spin splitting stems from the interfacial exchange coupling with the out-of-plane magnetized $CrCl_3$ layers, which disrupts the combined *PT* symmetry protecting spin degeneracy in the isolated $VSiS_3$ layer. Notably, the spontaneous valley polarization of 4.08 meV is preserved at the VBM for both states. The coexistence of valley spin splitting and valley polarization enables the observation of AVH effect in AFM $VSiS_3$ layer. The underlying physics of the observed spin-valley polarization can be attributed to the effective sublattice-asymmetric exchange fields acting on the V atoms in the central layer. As discussed above, this field arises from distinct magnetic exchange interactions experienced by each V sublattice, governed by their specific coordination with the spin-polarized $CrCl_3$ layers above and below. Crucially, as shown in Fig. 3, the valley spin splitting in the two states is opposite to each other. In state-I, the spin-down band resides at a higher energy than the spin-up band within the valence band, leading to spin-down polarization at the K valley. Conversely, in state-II, the spin polarization at each valley is reversed relative to state-I, resulting in spin-up polarization at the K valley. This controlled reversal of valley spin splitting between state-I and state-II demonstrates that the AVH signal generated in the AFM layer can be switched by reorienting the magnetization direction of the FM layers. The ability to magnetically toggle between state-I and state-II, facilitated by the low-energy barrier, offers a promising pathway for designing valleytronic devices with nonvolatile switching capabilities. While the calculated Curie temperature of monolayer $CrCl_3$ is indeed low (∼17 K) [46], it is important to emphasize that ordering temperatures of $CrCl_3$ monolayer can be substantially enhanced through various established experimental strategies such as substitutional doping or interface engineering [46–48]. Moreover, the proposed mechanism for achieving a switchable anomalous valley Hall effect is general and not restricted to the specific materials. The essential physics relies on a few key criteria: (i) the formation of a stable, lattice-matched heterotrilayer between the FM and AFM layers; (ii) the requirement that the band edges near the Fermi level are dominated by the valley-carrying electronic states of the AFM layer to ensure active valley participation; and (iii) the FM layers must be capable of inducing a substantial sublattice-asymmetric exchange field to break the combined *PT* symmetry of the AFM layer while preserving its intrinsic valley polarization. These criteria can be satisfied by a broader class of 2D materials. For instance, the FM layer $CrCl_3$ could be substituted by other 2D FM semiconductors with higher Curie temperatures, such as CrI_3 [49] or $CrGeTe_3$ [50]. Similarly, the AFM valley-active layer $VSiS_3$ could be replaced by other well-known 2D AFM semiconductors hosting valley properties, such as $MnPSe_3$ [51] or $FePS_3$ [52], in which the requisite valley physics and magnetic order are present. Therefore, our work establishes a general framework for achieving nonvolatile control of the valley Hall effect in antiferromagnets through interfacial design.

The Berry curvature, denoted as $\Omega(k)$, is a fundamental geometric property of electronic Bloch states in momentum space. Analogous to a magnetic field in real space, it governs

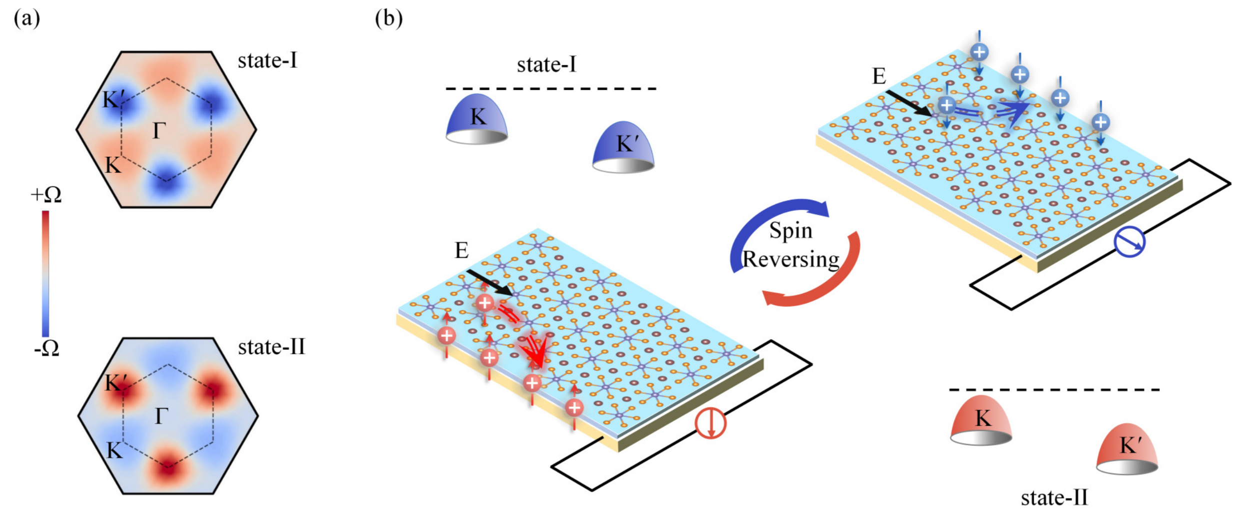

FIG. 4. (a) Berry curvatures of state-I and state-II. (b) Schematic diagram of AVHE of state-I and state-II.

the anomalous transverse velocity acquired by carriers under an applied electric field [53,54]. It is expressed as

$$\Omega(\mathrm{k}) = -\sum_{n}\sum_{n\neq n'} f_n \frac{2\mathrm{Im}\langle\psi_{nk}|v_x|\psi_{n'k}\rangle\langle\psi_{nk}|v_y|\psi_{n'k}\rangle}{(E_n - E_{n'})^2},$$

where f_n denotes the Fermi-Dirac distribution function, ψ_{nk} signifies the Bloch wave function with energy E_n, and v_x/v_y is the velocity operators of the x or y directions [55–58]. To access the impact of magnetic state switching on the AVHE, we calculate the Berry curvature distribution across the Brillouin zone for both state-I and state-II. As illustrated in Fig. 4(a), a key finding is the opposite signs of the Berry curvatures concentrated at the K valley between the two states. This sign reversal stems from the flipped valley spin splitting shown in Fig. 3.

The anomalous transverse velocity v of carriers is related to the Berry curvature and the applied in-plane electric field by $v \sim E \times \Omega(\mathrm{k})$ [59–61]. Consequently, carriers in valleys with opposite Berry curvatures are deflected to opposite transverse edges under the same in-plane electric field. As shown in Fig. 4(b), in state-I, holes at the K valley are predominantly spin-up polarized, and the positive Berry curvature at K valley deflects spin-up holes to acquire an anomalous velocity accumulating at the right transverse edge. While in state-II, the spin splitting at the K valley reverses, and the sign of the Berry curvature concurrently inverts to negative. Consequently, the spin-down polarized holes at K valley experience an anomalous velocity towards the left transverse edge. This magnetic-state-dependent reversal of both the valley spin splitting and Berry curvature at the K valley forms the basis for controllable AVHE in AFM layers. The low-energy barrier for coherent magnetic switching between state-I and state-II [Fig. 2(d)] confirms the feasibility of deterministic control over this AVHE sign reversal. To elucidate the anomalous Hall conductivity (AHC), we perform explicit calculations, as presented in Fig. S4 within the Supplemental Material [32]. The results exhibit a finite AHC with a sign reversal that aligns well with the Berry curvature distribution in Fig. 4(a). Notably, a fully valley-polarized Hall conductivity is achieved when the Fermi level lies between the K and K' valleys in the valence band. This behavior confirms the AVH effect in the $CrCl_3-VSiS_3-CrCl_3$ heterotrilayer, which can be probed via direct electrical transport measurements. Such experimental accessibility further supports the potential of this system for practical valleytronic applications.

III. CONCLUSIONS

In summary, we present an approach to achieve and manipulate the AVHE in AFM systems. By leveraging interfacial proximity effects in a tailored heterotrilayer, our calculations reveal that a robust, sublattice-asymmetric exchange field emerges, which breaks *PT* symmetry and lifts valley spin degeneracy while sustaining valley polarization, which is key to activating the AVHE. Most notably, this asymmetric field can be reversibly switched by reorienting the magnetization of the ferromagnetic layers, enabling nonvolatile control of the valley Hall signal without perturbing the antiferromagnetic order. Our work opens avenue for effective control of valley phenomena in antiferromagnets and significantly advances the prospects of valleytronic applications.

IV. METHODS

The first-principles calculations were performed using density functional theory (DFT) methods in the Vienna *Ab initio* Simulation Package (VASP) [62,63]. The exchange-correlation interactions were modeled with the Perdew-Burke-Ernzerhof (PBE) functional under the generalized gradient approximation (GGA) [64]. Strong electron correlation effects in 3*d* orbitals of V atom and Cr atom were described through an effective on-site Hubbard term of $U = 4$ eV, which refers to the previous work [30]. Structural optimizations were performed with the convergence criterion of 10^{-5} eV for the total energy and $0.01\,\mathrm{eV\,Å^{-1}}$ for the atomic forces. The cutoff energy is set to 520 eV. To eliminate the interactions between adjacent periodical structures, a 15 Å vacuum layer along the out-of-plane direction was established. A $9 \times 9 \times 1$ Monkhorst-Pack k-point grid was adopted to sample the Brillouin zone. For vdW interaction, we employed the DFT-D3 method with Becke-Johnson damping function. The calculation of phonon spectra was performed within the framework of density functional perturbation theory (DFPT), as implemented in the PHONOPY code [65]. The Berry curvature and valley Hall conductivity were obtained using the VASPBERRY code and WANNIER90 package [66–69].

ACKNOWLEDGMENTS

This work is supported by the National Natural Science Foundation of China (Grant No. 12274261), the Taishan Young Scholar Program of Shandong Province, and the Shandong Provincial Natural Science Foundation of China (Grant No. ZR2024QA016).

DATA AVAILABILITY

The data that support the findings of this article are not publicly available upon publication because it is not technically feasible and/or the cost of preparing, depositing, and hosting the data would be prohibitive within the terms of this research project. The data are available from the authors upon reasonable request.

[1] Q. Cui, Y. Zhu, J. Liang, P. Cui, and H. Yang, Spin-valley coupling in a two-dimensional VSi_2N_4 monolayer, Phys. Rev. B **103**, 085421 (2021).

[2] J. Zhao, Y. Qi, C. Yao, and H. Zeng, Tunable valley-spin splitting in a Janus $XMSiN_2$ monolayer (X = S, Se; M = Mo, Cr) and giant valley polarization via vanadium doping, Phys. Rev. B **109**, 035408 (2024).

[3] R. Ahammed and A. De Sarkar, Valley spin polarization in two-dimensional h-MN (M = Nb, Ta) monolayers: Merger of valleytronics with spintronics, Phys. Rev. B **105**, 045426 (2022).

[4] J. Yuan, Q. Wei, M. Sun, X. Yan, Y. Cai, L. Shen, and U. Schwingenschlögl, Protected valley states and generation of valley-and spin-polarized current in monolayer MA_2Z_4, Phys. Rev. B **105**, 195151 (2022).

[5] F. Bussolotti, T. D. Maddumapatabandi, and K. E. J. Goh, Band structure and spin texture of 2D materials for valleytronics: Insights from spin and angle-resolved photoemission spectroscopy, Mater. Quantum Technol. **3**, 032001 (2023).

[6] Y. Wang, H. Sun, C. Wu, W. Zhang, S. D. Guo, Y. She, and P. Li, Multifield tunable valley splitting and anomalous valley Hall effect in two-dimensional antiferromagnetic MnBr, Phys. Rev. B **111**, 085432 (2025).

[7] S. D. Guo, X. S. Guo, and G. Wang, Valley polarization in two-dimensional tetragonal altermagnetism, Phys. Rev. B **110**, 184408 (2024).

[8] S. A. Vitale, D. Nezich, J. O. Varghese, P. Kim, N. Gedik, P. Jarillo-Herrero, D. Xiao, and M. Rothschild, Valleytronics: Opportunities, challenges, and paths forward, Small **14**, 1801483 (2018).

[9] N. Rohling, M. Russ, and G. Burkard, Hybrid spin and valley quantum computing with singlet-triplet qubits, Phys. Rev. Lett. **113**, 176801 (2014).

[10] G. Y. Wu, N. Y. Lue, and L. Chang, Graphene quantum dots for valley-based quantum computing: A feasibility study, Phys. Rev. B **84**, 195463 (2011).

[11] N. Rohling and G. Burkard, Universal quantum computing with spin and valley states, New J. Phys. **14**, 083008 (2012).

[12] J. Isberg, M. Gabrysch, J. Hammersberg, S. Majdi, K. K. Kovi, and D. J. Twitchen, Generation, transport and detection of valley-polarized electrons in diamond, Nat. Mater. **12**, 760 (2013).

[13] C. S. Boland, Y. Sun, and D. G. Papageorgiou, Bandgap engineering of 2D materials toward high-performing straintronics, Nano Lett. **24**, 12722 (2024).

[14] A. Soni and S. K. Pal, Valley degree of freedom in two-dimensional van der Waals materials, J. Phys. D Appl. Phys. **55**, 303003 (2022).

[15] J. R. Schaibley, H. Yu, G. Clark, P. Rivera, J. S. Ross, K. L. Seyler, W. Yao, and X. Xu, Valleytronics in 2D materials, Nat. Rev. Mater. **1**, 16055 (2016).

[16] G. Pacchioni, Valleytronics with a twist, Nat. Rev. Mater. **5**, 480 (2020).

[17] C. Luo, Z. Huang, H. Qiao, X. Qi, and X. Peng, Valleytronics in two-dimensional magnetic materials, J. Phys. Mater. **7**, 022006 (2024).

[18] L. Li, L. Shao, X. Liu, A. Gao, H. Wang, B. Zheng, G. Hou, K. Shehzad, L. Yu, F. Miao, *et al.*, Room-temperature valleytronic transistor, Nat. Nanotechnol. **15**, 743 (2020).

[19] X. Wang, L. Liu, N. Wang, Y. Chen, T. Song, Z. Liu, and X. Cui, First-principles study on valley polarization of ferromagnetic $PrBr_2$ monolayer under strain, J. Phys. Chem. C **128**, 6897 (2024).

[20] W. Y. Tong, S. J. Gong, X. Wan, and C. G. Duan, Concepts of ferrovalley material and anomalous valley Hall effect, Nat. Commu. **7**, 13612 (2016).

[21] S. D. Guo, P. Li, and G. Wang, Proposal of a general scheme: Valley polarization in antiferromagnetic bilayer systems, arXiv:2411.06454.

[22] S. D. Guo, Y. L. Tao, Z. Y. Zhuo, G. Zhu, and Y. S. Ang, Electric-field-tuned anomalous valley Hall effect in A-type hexagonal antiferromagnetic monolayers, Phys. Rev. B **109**, 134402 (2024).

[23] S. D. Guo, L. Zhang, Y. Zhang, P. Li, and G. Wang, Large spontaneous valley polarization and anomalous valley Hall effect in antiferromagnetic monolayer Fe_2CF_2, Phys. Rev. B **110**, 024416 (2024).

[24] Y. Zhu, J. T. Sun, J. Pan, J. Deng, and S. Du, Enforced symmetry breaking for anomalous valley Hall effect in two-dimensional hexagonal lattices, Phys. Rev. Lett. **134**, 046403 (2025).

[25] B. Zhang, F. Zheng, X. Chen, F. Deng, and J. Wang, Anomalous valley Hall effect induced by sublattice symmetry breaking in ABX_3 honeycomb kagomé lattice, Phys. Rev. B **108**, 045146 (2023).

[26] X. Li, T. Cao, Q. Niu, J. Shi, and J. Feng, Coupling the valley degree of freedom to antiferromagnetic order, Proc. Natl. Acad. Sci. USA **110**, 3738 (2013).

[27] X. X. Zhang, Y. Lai, E. Dohner, S. Moon, T. Taniguchi, K. Watanabe, D. Smirnov, and T. F. Heinz, Zeeman-induced

valley-sensitive photocurrent in monolayer MoS_2, Phys. Rev. Lett. **122**, 127401 (2019).

[28] K. F. Mak, K. He, J. Shan, and T. F. Heinz, Control of valley polarization in monolayer MoS_2 by optical helicity, Nat. Nanotechnol. **7**, 494 (2012).

[29] H. Zeng, J. Dai, W. Yao, D. Xiao, and X. Cui, Valley polarization in MoS_2 monolayers by optical pumping, Nat. Nanotechnol. **7**, 490 (2012).

[30] B. L. Chittari, D. Lee, N. Banerjee, A. H. MacDonald, E. Hwang, and J. Jung, Carrier- and strain-tunable intrinsic magnetism in two-dimensional MAX_3 transition metal chalcogenides, Phys. Rev. B **101**, 085415 (2020).

[31] L. Webster and J. A. Yan, Strain-tunable magnetic anisotropy in monolayer $CrCl_3$, $CrBr_3$, and CrI_3, Phys. Rev. B **98**, 144411 (2018).

[32] See Supplemental Material at http://link.aps.org/supplemental/10.1103/bdfy-8ff7 for the details regarding the phonon spectra of monolayer $CrCl_3$ and $VSiS_3$ as well as the $CrCl_3-VSiS_3-CrCl_3$ heterotrilayer, the relaxed crystal structure and *ab initio* molecular dynamics simulations of the heterotrilayer at room temperature, the energy comparison among different $CrCl_3-VSiS_3-CrCl_3$ heterotrilayers, and the anomalous Hall conductivity of the ground state configuration.

[33] M. Velický, P. S. Toth, A. M. Rakowski, A. P. Rooney, A. Kozikov, C. R. Woods, A. Mishchenko, L. Fumagalli, J. Yin, V. Zolyomi, *et al.*, Exfoliation of natural van der Waals heterostructures to a single unit cell thickness, Nat. Commun. **8**, 14410 (2017).

[34] R. K. Barik and L. M. Woods, High throughput calculations for a dataset of bilayer materials, Sci. Data **10**, 232 (2023).

[35] T. N. Do, S. T. Nguyen, and C. Q. Nguyen, Adjusting the electronic properties and contact types of graphene/F-diamane-like C_4F_2 van der Waals heterostructure: A first-principles study, RSC Adv. **11**, 37981 (2021).

[36] X. Xu, L. Yang, Q. Gao, X. Jiang, D. Li, B. Cui, and D. Liu, Type-II $MoSi_2N_4/MoS_2$ van der Waals heterostructure with excellent optoelectronic performance and tunable electronic properties, J. Phys. Chem. C **127**, 7878 (2023).

[37] K. Jiang, J. Ji, W. Gong, L. Ding, J. Li, P. Li, B. Li, and F. Geng, Mechanical cleavage of non-van der Waals structures towards two-dimensional crystals, Nat. Synth. **2**, 58 (2023).

[38] J. Wang, Z. Ahmadi, D. Lujan, J. Choe, T. Taniguchi, K. Watanabe, X. Li, J. E. Shield, and X. Hong, Physical vapor transport growth of antiferromagnetic $CrCl_3$ flakes down to monolayer thickness, Adv. Sci. **10**, 2203548 (2023).

[39] Y. Cao, A. Mishchenko, G. L. Yu, E. Khestanova, A. P. Rooney, E. Prestat, A. V. Kretinin, P. Blake, M. B. Shalom, C. Woods, *et al.*, Quality heterostructures from two-dimensional crystals unstable in air by their assembly in inert atmosphere, Nano Lett. **15**, 4914 (2015).

[40] V. Patil, S. Ghosh, A. Basu, A. Dutta Kuldeep, K. Agrawal, N. Bhatia, A. Shah, D. A. Jangade, R. Kulkarni, A. Thamizhavel, and M. M. Deshmukh, Pick-up and assembling of chemically sensitive van der Waals heterostructures using dry cryogenic exfoliation, Sci. Rep. **14**, 11097 (2024).

[41] F. Pizzocchero, L. Gammelgaard, B. S. Jessen, J. M. Caridad, L. Wang, J. Hone, P. Boggild, and T. J. Booth, The hot pick-up technique for batch assembly of van der Waals heterostructures, Nat. Commun. **7**, 11894 (2016).

[42] F. Yang, Y. Ji, X. Li, Y. Dai, B. Huang, and Y. Ma, Anomalous valley Hall effect in two-dimensional *p*-orbital honeycomb lattice, Appl. Phys. Lett. **126**, 252404 (2025).

[43] X. Liang, Y. Liu, T. Zhong, T. Yang, J. Li, L. Luo, G. Dong, Y. Chen, X. Luo, T. Tang, and L. Bi, Mechanisms of manipulating valley splitting in $MoTe_2/MnS_2$ van der Waals heterostructure by electric field and strains, RSC Adv. **14**, 10209 (2024).

[44] F. Sattari and S. Mirershadi, Effect of the strain on spin-valley transport properties in MoS_2 superlattice, Sci. Rep. **11**, 17617 (2021).

[45] M. U. Farooq and J. Hong, Switchable valley splitting by external electric field effect in graphene/CrI_3 heterostructures, npj 2D Mater. Appl. **3**, 3 (2019).

[46] F. Xue, Y. Hou, Z. Wang, and R. Wu, Two-dimensional ferromagnetic van der Waals $CrCl_3$ monolayer with enhanced anisotropy and Curie temperature, Phys. Rev. B **100**, 224429 (2019).

[47] D. Mastrippolito, J. Wang, G. Profeta, and L. Ottaviano, Unconventional ferrimagnetism and enhanced magnetic ordering temperature in monolayer $CrCl_3$ by introducing O impurities and Cl vacancies, J. Phys. Mater. **5**, 014004 (2022).

[48] Ł. Kipczak, Z. Chen, M. Grzeszczyk, S. Grebenchuk, P. Huang, K. Vaklinova, K. Watanabe, T. Taniguchi, A. Babinski, M. Koperski, and M. R. Molas, Interplay between charge transfer and magnetic proximity effects in $WSe_2/CrCl_3$ heterostructures, Nanoscale Horiz. **10**, 2465 (2025).

[49] C. Gong, L. Li, Z. Li, H. Ji, A. Stern, Y. Xia, T. Cao, W. Bao, C. Wang, Y. Wang, *et al.*, Discovery of intrinsic ferromagnetism in two-dimensional van der Waals crystals, Nature (London) **546**, 265 (2017).

[50] B. Huang, G. Clark, E. Navarro-Moratalla, D. R. Klein, R. Cheng, K. L. Seyler, D. Zhong, E. Schmidgall, M. A. McGuire, D. H. Cobden, *et al.*, Layer-dependent ferromagnetism in a van der Waals crystal down to the monolayer limit, Nature (London) **546**, 270 (2017).

[51] B. Jhun and C. H. Park, Electronic structure of charged bilayer and trilayer phosphorene, Phys. Rev. B **96**, 085412 (2017).

[52] A. P. Schlaus, M. S. Spencer, K. Miyata, F. Liu, X. Wang, I. Datta, M. Lipson, A. Pan, and X. Y. Zhu, How lasing happens in $CsPbBr_3$ perovskite nanowires, Nat. Commun. **10**, 265 (2019).

[53] N. Nagaosa, J. Sinova, S. Onoda, A. H. MacDonald, and N. P. Ong, Anomalous Hall effect, Rev. Mod. Phys. **82**, 1539 (2010).

[54] M. C. Chang and Q. Niu, Berry curvature, orbital moment, and effective quantum theory of electrons in electromagnetic fields, J. Phys.: Condens. Matter **20**, 193202 (2008).

[55] D. J. Thouless, M. Kohmoto, M. P. Nightingale, and M. den Nijs, Quantized Hall conductance in a two-dimensional periodic potential, Phys. Rev. Lett. **49**, 405 (1982).

[56] M. Gradhand, D. V. Fedorov, F. Pientka, P. Zahn, I. Mertig, and B. L. Györffy, First-principle calculations of the Berry curvature of Bloch states for charge and spin transport of electrons, J. Phys.: Condens. Matter **24**, 213202 (2012).

[57] C. C. Lee, Y. T. Lee, M. Fukuda, and T. Ozaki, Tight-binding calculations of optical matrix elements for conductivity using nonorthogonal atomic orbitals: Anomalous Hall conductivity in bcc Fe, Phys. Rev. B **98**, 115115 (2018).

[58] G. Jin, D. Zheng, and L. He, Calculation of Berry curvature using non-orthogonal atomic orbitals, J. Phys.: Condens. Matter **33**, 325503 (2021).

[59] D. Xiao, M. C. Chang, and Q. Niu, Berry phase effects on electronic properties, Rev. Mod. Phys. **82**, 1959 (2010).

[60] Y. Araki and J. I. Ieda, Intrinsic torques emerging from anomalous velocity in magnetic textures, Phys. Rev. Lett. **127**, 277205 (2021).

[61] L. Xiang and J. Wang, Intrinsic in-plane magnetononlinear Hall effect in tilted Weyl semimetals, Phys. Rev. B **109**, 075419 (2024).

[62] G. Kresse and J. Furthmüller, Efficient iterative schemes for *ab initio* total-energy calculations using a plane-wave basis set, Phys. Rev. B **54**, 11169 (1996).

[63] W. Kohn and L. J. Sham, Self-consistent equations including exchange and correlation effects, Phys. Rev. **140**, A1133 (1965).

[64] J. P. Perdew, K. Burke, and M. Ernzerhof, Generalized gradient approximation made simple, Phys. Rev. Lett. **77**, 3865 (1996).

[65] S. Mann, P. Rani, R. Kumar, and V. K. Jindal, DFT study of phonon dispersion in pure graphene, AIP Conf. Proc. **1675**, 030035 (2015).

[66] T. Zhang, X. Xu, B. Huang, Y. Dai, L. Kou, and Y. Ma, Layer-polarized anomalous Hall effects in valleytronic van der Waals bilayers, Mater. Horiz. **10**, 483 (2023).

[67] R. Peng, T. Zhang, Z. He, Q. Wu, Y. Dai, B. Huang, and Y. Ma, Intrinsic layer-polarized anomalous Hall effect in bilayer $MnBi_2Te_4$, Phys. Rev. B **107**, 085411 (2023).

[68] J. Luo, H. Meng, X. X. Xue, K. Q. Chen, and L. M. Tang, Intrinsic ferrovalley non-Janus FeXI (X = Cl, Br) with large valley polarization and nonvolatile reversible control of the anomalous valley Hall effect in multiferroic heterojunctions, Phys. Rev. B **110**, 085401 (2024).

[69] A. A. Mostofi, J. R. Yates, Y.-S. Lee, I. Souza, D. Vanderbilt, and N. Marzari, WANNIER90: A tool for obtaining maximally localised Wannier functions, Comput. Phys. Commun. **178**, 685 (2008).